Growth Mechanism of Chevron Graphene Nanoribbons on (111)-Oriented Coinage Metal Surfaces

Elie Geagea, Daniel Medina-Lopez, Luca Giovanelli, Laurent Nony, Christian Loppacher, Stéphane Campidelli, Sylvain Clair

Growth Mechanism of Chevron Graphene Nanoribbons on (111)-Oriented Coinage Metal Surfaces

Elie Geagea[1], Daniel Medina-Lopez[2], Luca Giovanelli[1], Laurent Nony[1], Christian Loppacher[1], Stéphane Campidelli[2], Sylvain Clair[1,*]

[1] *Aix Marseille University, CNRS, IM2NP, Marseille, France*

[2] *Université Paris-Saclay, CEA, CNRS, NIMBE, LICSEN, 91191, Gif-sur-Yvette, France*

*Corresponding author: sylvain.clair@cnrs.fr

Abstract

Atomically precise on-surface synthesis of graphene nanoribbons (GNR) with well-defined width and edge configuration has been widely advanced during the last decade. The main bottom-up growth strategy relies on the thermally activated Ullmann-like coupling reaction followed by the cyclodehydrogenation of tailor-made precursors to achieve the desired precision. We present a systematic investigation of the growth mechanism of chevron GNR on the Ag(111), Au(111) and Cu(111) surfaces in ultrahigh vacuum (UHV). We found that the multistep reaction follows different pathways with different activation temperatures depending on the supporting surface. The importance of the as-released Br and their potential influence on the growth process are discussed. The different intermediate states were investigated by low-temperature Scanning Tunneling Microscopy in combination with Thermal Desorption Spectroscopy and Kinetic Monte Carlo simulations.

Introduction

On-surface synthesis has been established in recent years as an efficient approach to create atomically-defined organic compounds and nanostructures.[1-5] Among the latter, graphene nanoribbons (GNR)[6] have attracted particularly high attention due to their exceptional properties, the atomic-scale control on their structure and their smooth integration into electronic devices.[1,7-10] GNR are usually obtained from the surface-supported Ullmann-like coupling of specially designed di-halogenated precursors. The growth of GNR is easiest on metal surfaces, where the precise nature and crystallographic orientation of the substrate play a dominant role in the growth process and even in the structure of the final product.[11-13]

While armchair GNRs (aGNR), and in particular 7-aGNR[6] obtained from 10,10'-dibromo-9,9'-bianthracene, represent by far the most studied GNR type, chevron GNRs (cGNR) based on 6,11-dibromo-1,2,3,4-tetraphenyltriphenylene (precursor **1**, Fig. 1) have also attracted particular attention. They have been extensively studied experimentally as well as theoretically,[6,14-32] also by considering atomic modifications such as the introduction of heteroatoms[28-38] or the addition of bulky edge groups.[25-27,39-44] While most of these works highlight the interest of GNR as a final product, the on-surface growth process and the different intermediate states leading to the GNR formation have been only scarcely studied and rarely systematically addressed.

Ullmann-like coupling reactions of halogenated compounds in on-surface synthesis occurs through different thermally activated steps: the dehalogenation, the formation of an organometallic intermediate and the final C-C coupling. On Au(111), however, the organometallic usually does not form[45-48] except in rare cases.[49,50] For GNR, an additional final step is occurring at higher annealing temperature, an extended cyclodehydrogenation reaction, leading to the planarization and aromatization of the ribbons. The atomic structure of the GNR can be precisely elucidated with the help of scanning probe microscopy (SPM) images, and the intermediate steps can be traced back by SPM and photoelectron spectroscopy (XPS) measurements. In addition, thermal desorption spectroscopy (TDS), also called temperature-programmed desorption (TPD) or temperature-programmed reaction spectroscopy (TPRS) can provide further insights into the growth mechanism.[51-54] It was thus shown that on Au(111) the bromine byproduct desorbs from the surface in the form of HBr during the cyclodehydrogenation phase.[55-57]

In this article we performed systematic comparative investigations of the growth mechanism of chevron GNR on the Ag(111), Au(111) and Cu(111) surfaces in ultrahigh vacuum (UHV) using low-temperature scanning probe microscopy (LT-STM) and TDS measurements. We found various processes that have not been observed before or that were at least largely overlooked. Different kinds of supramolecular interactions due to different chain intertwining are found between the intermediate organometallic and between the polymeric chains. On Au(111) an additional intermediate state forms due to partial

dehydrogenation. The final cyclodehydrogenation mechanism appears different on Cu(111) as compared to Au(111) and Ag(111). Finally, the role of co-adsorbed Br in the growth mechanism is pointed out, in particular in the case of Cu(111) where it does not desorb from the surface.

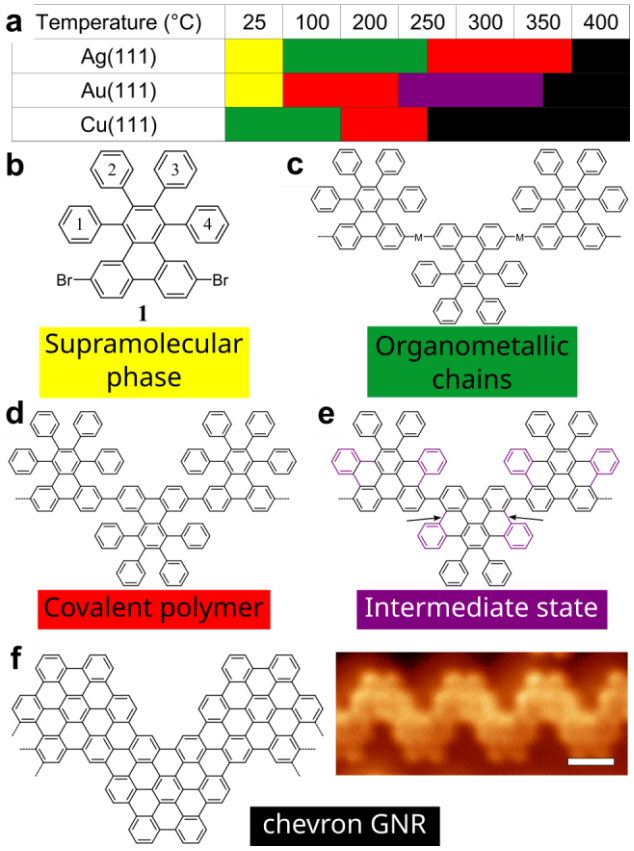

Fig. 1. (a) Overview of the evolution of the intermediate structures, symbolized by a color code, that are obtained upon annealing at different temperatures. (b) Molecular precursor **1**, its pristine form is found in the supramolecular phase (yellow). (c) Organometallic chains (green). (d) Covalent polymer (red). (e) Intermediate state on Au(111) (purple) , the new bonds are indicated by the arrows. (f) Final chevron GNR (black) and corresponding STM image. Scale bar: 1 nm.

Methods

The GNR precursor **1** (6,11-dibromo-1,2,3,4-tetraphenyltriphenylene)[6] was synthesized according to the literature procedure,[38,58] see details in SI.

The experiments were performed in an ultrahigh vacuum (UHV) setup consisting of a preparation chamber for sample cleaning, molecular deposition and desorption experiments, and an analysis chamber for low-temperature scanning tunneling microscopy (Scienta Omicron Infinity LT-STM, T = 9.5 K). The molecular precursor was evaporated on the substrate at room temperature (when not

otherwise stated) from a crucible heated at 175 °C providing a flux of about 0.03 ML/min. Annealing was performed at the indicated temperatures for 10 min. The LT-STM experiments were carried out in constant-current mode with the voltage applied to the sample (typical values I = 50 pA, V = -1.3 to +1.3 V) using a Nanonis RC5 electronic controller. The images were analyzed using the WSxM[59] and SPIP 6 softwares.

The conformation of the molecular models superimposed on the STM images in Figs. 2,3 and Fig. S2 is arbitrary, no computational relaxation was performed. DFT simulations of different related structures can be found in previous work.[6,17,19,24,31]

In TDS experiments, the quadrupole mass spectrometer (Pfeiffer PrismaPro) was brought just above the sample surface and the annealing was performed with a linearly increasing heating current intensity providing a nearly stable heating rate of 20 $K.min^{-1}$. The base pressure was ~1.10^{-9} mbar. Masses 2 and 82 were recorded corresponding to the desorption of H_2 and HBr, respectively. The ratio of mass 82 to mass 81 was found identical for the Ag(111) and Au(111) cases. The same results are obtained when considering the second ^{79}Br isotope and the masses 80 and 79.

The TDS results were modelled using Kinetic Monte Carlo methods implemented in CARLOS program,[60,61] see SI for details.

Results

The precursor for chevron GNR growth is 6,11-dibromo-1,2,3,4-tetraphenyltriphenylene (molecule **1**, Fig. 1b). It is composed of a triphenylene core with four substituted phenyls, providing high flexibility due to the free rotations along the C-C single bonds. After deposition in UHV, the precursor is imaged by LT-STM with the main contrast consisting of four bright lobes corresponding to the four rotating phenyls (see Fig. 2e). In the supramolecular phase of **1**,[23,24] the molecules are adsorbed in their pristine form on the surface and self-assemble through π-π interactions between the phenyl groups.[24] The supramolecular phase is observed after room-temperature deposition on Au(111) and on Ag(111) (see SI Fig. S1a-d). In the case of Ag(111), there is the possibility of a partial debromination of the precursors, similar to what has been observed for other brominated precursors.[13,46] On Cu(111) the debromination reaction occurs usually at temperatures lower than RT. It was measured at a temperature of about -30 °C in the case of armchair GNR.[11] We could observe accordingly the supramolecular phase on Cu(111) after deposition on the surface kept at -80 °C (SI Fig. S1e,f).

Organometallic chains

On Cu(111) after room temperature deposition and up to an annealing temperature of 100 °C, the formation of one-dimensional (1D) organometallic chains is observed (Fig. 2). The periodicity along the chains is 2.22 ± 0.05 nm (see SI Table S1). The chains are lying in close vicinity to each other forming two dimensional (2D) domains. The attractive lateral interaction between the chains is given by the formation of π-π supramolecular bonding interactions.[6] Three different supramolecular configurations of the organometallic chains coexist. Noticeably, the two dominant ones (Fig. 2b,c) are driven mainly by the π-π interaction between the phenyl rings labelled 2 and 3 of two neighboring chains (see Fig. 1b for the labelling of the phenyls). They slightly differ depending on whether the π-π interaction is achieved at the very edge of the chains (Fig. 2b) or laterally (Fig. 2c). As a result, the chains are slightly farther apart in the first configuration (1.85 ± 0.05 nm) than they are in the second (1.62 ± 0.05 nm). The third configuration (Fig. 2d) is more compact due to the complete intertwining of the two adjacent chains. In this case, the 2D assembly involves the π-π interaction between the phenyl rings labelled 2 and 3 and also between those labelled 1 and 4, and the distance between two chains shrinks to 1.32 ± 0.05 nm.
Similar organometallic chains are found on Ag(111) after annealing in the temperature range of 100 °C to 250 °C (see SI Fig. S2). The same three types of 2D supramolecular domain configurations were observed on the Ag(111) and on the Cu(111) surfaces, thus revealing the molecule-molecule interactions as the main driving forces for the 2D self-assembly of the chains, rather independently of the underlying substrate.

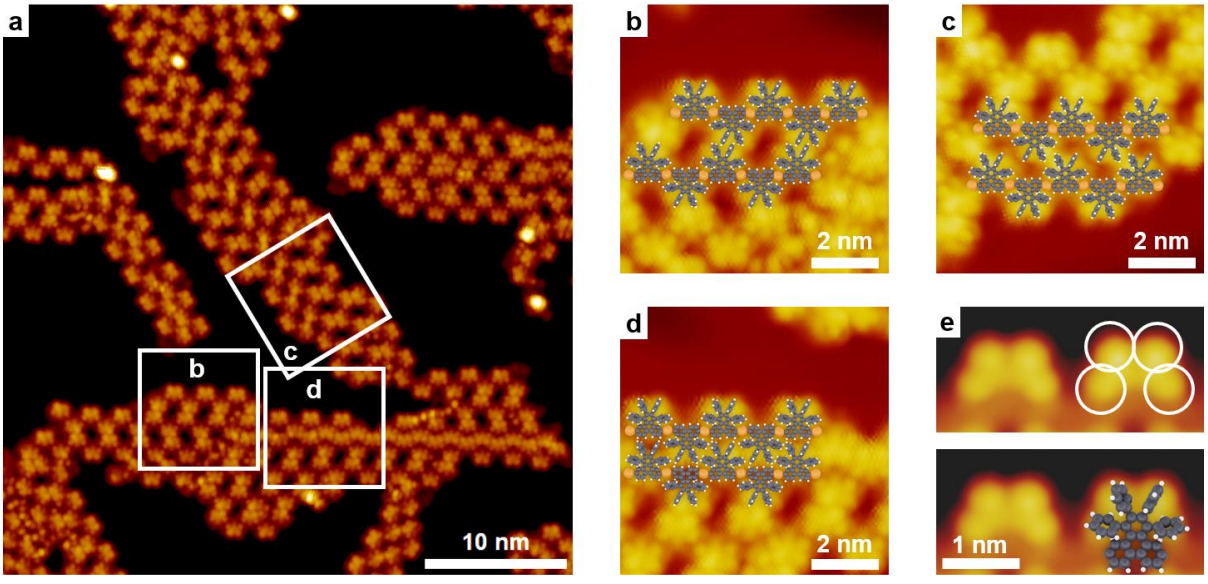

Fig. 2. STM images of the organometallic chains obtained on Cu(111) after annealing at 100 °C. (a) STM image representing the three distinct modes of 2D self-assembly highlighted with three white inspection areas corresponding to: (b,c) The two nanoporous phases are driven mainly by π-π

interactions between the two phenyls labelled 2 and 3 in Fig. 1; (d) A more compact structure resulting from an important chain intertwining and π-π interactions involving all four phenyls. Each interchain configuration is represented by a model superimposed on the STM images (scaled but not computationally fully relaxed). Carbon atoms: dark grey; Hydrogen atoms: white; Copper adatoms: yellow. (e) Detail STM image showing the typical contrast observed for the molecular precursor with the four lobes highlighted by the white circles and assigned to the four freely rotating phenyl groups.

Covalent polymers

On Au(111) the organometallic chains are not observed, as is usually the case in Ullmann-like reactions,[12,45-47] except in rare cases.[49,50] Annealing to 100 °C produces directly the formation of a covalent polymer through the formation of C-C bonds between the precursors, see Fig. 3b,e. The periodicity along the 1D polymer chains is 1.70 ± 0.05 nm (see SI Table S1). Here also, the chains self-assemble into 2D-like domains through lateral π-π interactions involving the phenyl rings labelled 2 and 3 on the edges of the polymeric chain. The distance between the parallel chains is equal to 1.65 ± 0.05 nm. The covalent chains are stable up to an annealing temperature of 300 °C. No structural difference could be observed by STM in the temperature range 100 °C to 300 °C. However, a minor chemical modification occurs between 200 °C and 250 °C, as described in the text below (partial dehydrogenation and formation of the intermediate state shown in Fig. 1e).

Similar covalent chains are observed on Ag(111) and Cu(111), see Fig 3. On Ag(111) the polymer is formed at an annealing temperature of 250 °C. Noticeably, only one domain type remains with an interchain distance of 1.65 ± 0.05 nm. On Cu(111) the polymer is formed at an annealing temperature of 200 °C. Here, two distinct arrangements still coexist, with interchain distances of 1.65 ± 0.05 nm and 1.90 ± 0.05 nm.

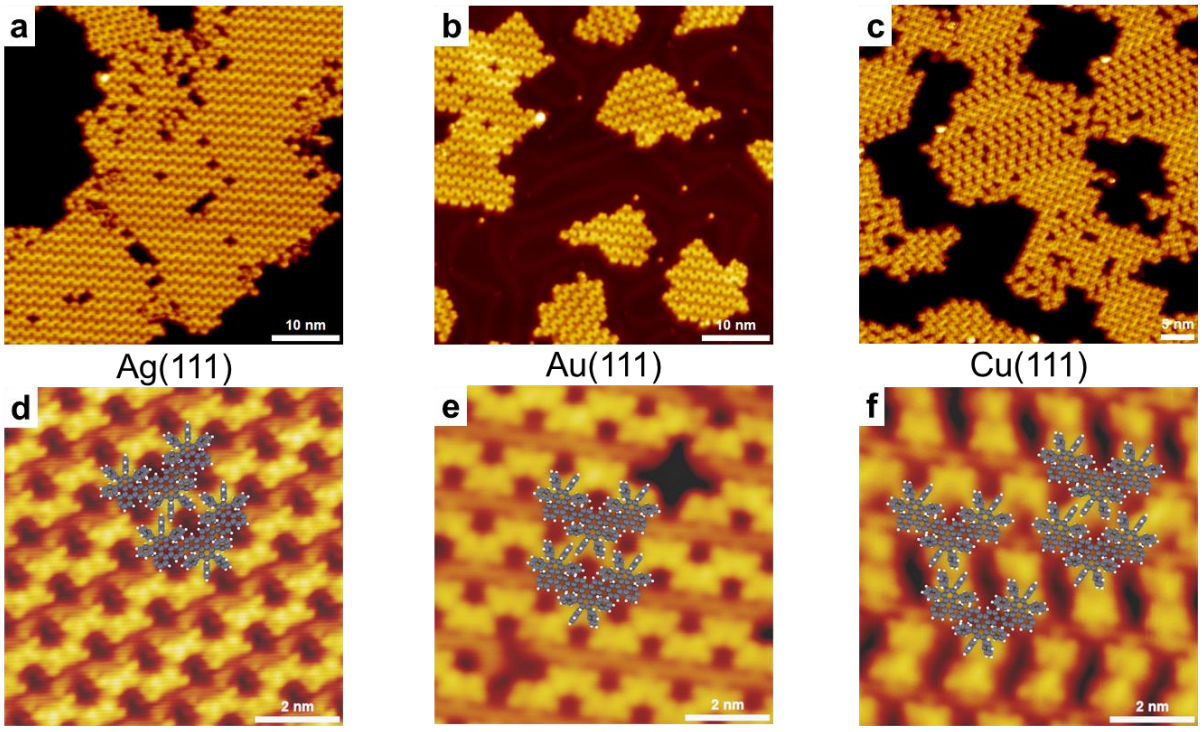

Fig. 3. STM images showing the domains of the covalent polymers obtained after annealing on (a) Ag(111) at 300 °C, (b) Au(111) at 200 °C and (c) Cu(111) at 200 °C. (d,e) On the Ag(111) and Au(111) surfaces, the polymer chains arrange into one similar domain type, as represented by the superimposed models. f) On Cu(111), two interchain interaction types coexist. On Au(111) the intermediate state obtained at higher annealing temperature presents the same organization (see SI Fig. S7). Each phase is represented by a model superimposed on the STM images (scaled but not computationally fully relaxed). Carbon atoms: dark grey; Hydrogen atoms: white.

GNR formation

The transition from the compact 2D-like domains of the covalent polymer phase to the GNR phase can be precisely observed by annealing at specific temperatures, i.e. 375 °C on Ag(111), 350 °C on Au(111) and 250 °C on Cu(111) (Fig. 4). Here, the local cyclodehydrogenation reactions between adjacent phenyl rings can be well identified by the STM contrast change, from bright dots on the protruding (rotated out-of-plane) non-reacted phenyls to the low homogeneous aromatic contrast of the planar cyclized groups.[62-65] Surprisingly, two different mechanisms take place. On Cu(111), the two peripheral phenyls labelled 2 and 3 (Fig. 4e) fuse first, while on Ag(111) and Au(111) the cyclodehydrogenation occurs first for a phenyl pair labelled 1,2 or 3,4 (Fig. 4d). On Cu(111) the planarization of the GNR is also accompanied by the appearance of bright protrusions in their vicinity that can be attributed to Br adatoms

(see SI Fig. S3). The different behaviors observed between the three surfaces during the cyclodehydrogenation process will be discussed below.

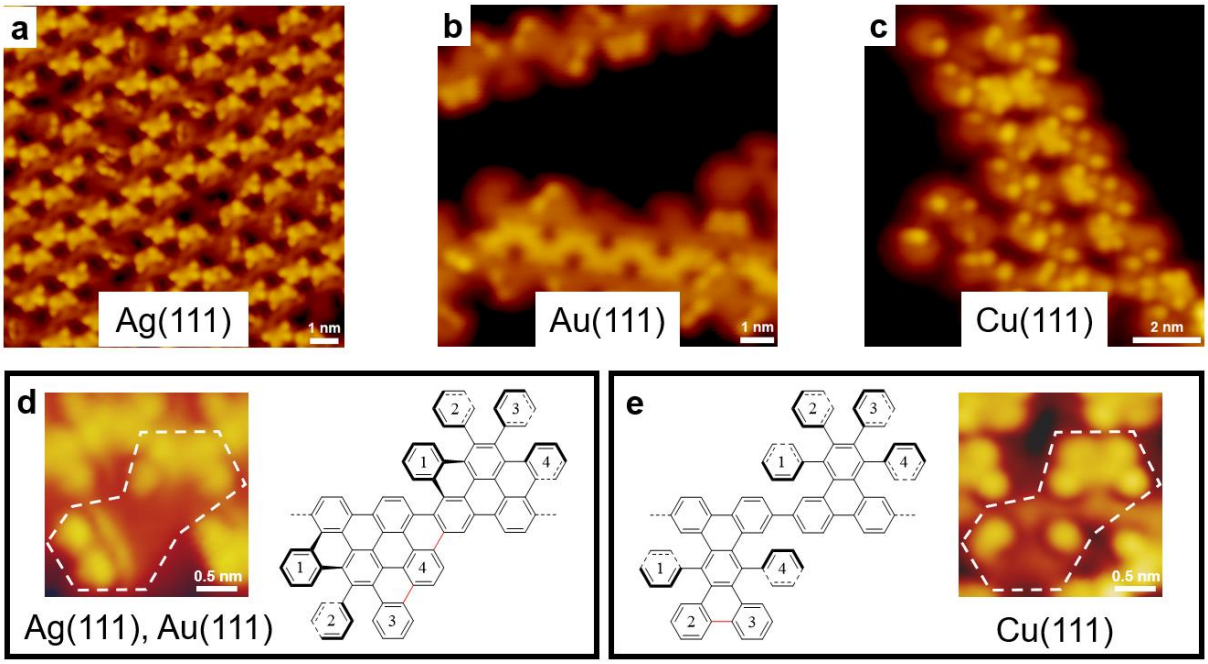

Fig. 4. STM images showing the transition steps to the GNR formation with an intermediate advancement of the cyclodehydrogenation reaction. On Ag(111) (a) and Au(111) (b) the cyclodehydrogenation occurs first through a 1,2 or 3,4 phenyl pair (d), and on Cu(111) (c) through the peripheral phenyls labelled 2 and 3 first (e). The newly formed bonds are highlighted in red. In scheme (e), the transition is shown from the covalent polymer (Fig. 1d), and in scheme (d) from the intermediate state as observed on Au(111) (Fig. 1e).

At high annealing temperature, full cyclodehydrogenation of the polymer chains occurs, leading to the formation of planar fully aromatic chevron-GNR. The required temperature is 400 °C on Ag(111) and on Au(111), and 300 °C on Cu(111). After GNR formation the surface morphology changes drastically. While the polymer chains are organized in compact 2D-like domains, the GNR are observed mostly in isolated form with well-defined separation distances (Fig. 5a and SI Fig. S4). This issue can also be observed in previously published STM images of cGNR.[17,19,23,29] Remarkably, the homogeneous separation of the ribbons seems to be quite general also for other CH-terminated GNRs,[34,39,52,66] and in particular for armchair GNR,[6,13,67] although such effect has never really been explicitly emphasized. On Au(111) the native herringbone surface reconstruction has been proposed as responsible for the long-range interaction,[66] but another driving force certainly also takes place because of the similar behavior

found on the Ag(111) and Cu(111) surfaces. In fact, repulsive intermolecular interaction is usually encountered on a metal surface between small polyaromatic molecules such as naphthalene,[68] tetracene,[69] perylene,[70] coronene,[71] hexabenzocoronene[72] or porphyrin.[73] Electrostatic repulsion could arise through two different effects: the dipole-dipole interaction due to the charge transfer to the surface,[74,75] or the polarization of the C-H bond as suggested for polyarenes.[69,70,72] Because of their large size extending over several substrate atomic periodicities, GNRs cannot adsorb with exact epitaxial coincidence and they exhibit superlubricity behavior.[76] The metal surface-GNR friction force was estimated to be in the range of 10 to 100 pN.[76] For comparison, two charges of 0.1 e^- at a distance of 1 nm apart exert a repulsion force of 2 pN. When added along the full GNR length, the electrostatic interaction easily reaches the order of magnitude of the friction force. Note that the GNR repulsion does not occur in the case of heteroatom-functionalized GNR at their edges.[37,38,77]

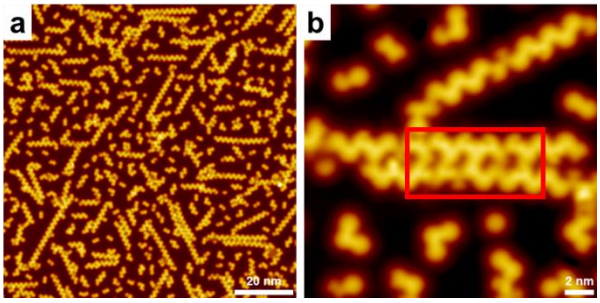

Fig. 5. STM images of chevron-GNR obtained on Ag(111) after annealing at 400 °C. (a) Large scale image showing the nanoribbon distribution in isolated form. (b) Zoom-in on a rare structure where two neighboring GNRs are locally fused.

Finally, due to the repulsive interaction appearing during the GNR formation, lateral fusion of the GNR is made very difficult and can be observed only scarcely (Fig. 5b and SI Fig. S5).[24] The full cyclodehydrogenation occurs first at the domain boundaries where the newly formed GNR can diffuse freely and withdraw from the domains, thus strongly restraining the possibility for a fusion reaction. In the eventuality of such withdrawing displacement being restrained due to an unfavorable arrangement of the GNR (hindered position or local disorder), defects can be formed locally in the form of individual phenyl losses (see SI Fig. S6), as it was also observed in Ref.[27] Interestingly, such defects were observed only on Ag(111) and Au(111), never on Cu(111). This may be related to the different mechanisms for the cyclodehydrogenation reaction occurring on Cu(111) (fusion of the phenyls labelled 2 and 3 first, see Fig. 4) as opposed to Ag(111) and Au(111), as it will be discussed below.

TDS analysis

In the last part, we performed thermal desorption measurements to gain further insights into the growth mechanism. For the general case of Ullmann-like reactions on Au(111), Br desorbs at relatively low temperature (230 °C to 280 °C) when there is no cyclodehydrogenation side-reaction such as for the formation of polyphenylene[46,78,79] or alike.[80] Otherwise, Br was shown to desorb in the form of molecular HBr at higher temperature (~350 °C), corresponding to the activation of the cyclodehydrogenation reactions,[55-57] which can be understood considering the higher interaction of adsorbed Br with the non-planar precursors.[55] Only one report mentions the desorption of Br at 250 °C observed by XPS for bianthracenyl precursors,[81] but the possibility of hydrogen contamination from the UHV chamber cannot be excluded.[82]

The TDS spectra for the formation of cGNR are shown in Fig. 6. On Ag(111), the HBr desorption peak is observed at 350 °C (Fig. 6a), corresponding to the transition temperature from the covalent polymer to the GNR, as observed by STM. The formation of HBr originates from the on-surface combination of adsorbed Br with the hydrogen released by the cyclodehydrogenation reaction. This peak is followed by a H_2 desorption peak due to the over-stoichiometry of the hydrogen released with respect to the amount of Br (H:Br ratio of 6:1), as shown previously.[55-57] HBr desorption occurs first because the rate-limiting step is the H release, and the HBr formation is of first-order kinetics whereas the H_2 formation is of second-order.[46,55,57] In the spectrum of Fig. 6a, there is a notable overlap between the HBr and the H_2 desorption peaks, while in the case of aGNR formation it was observed that both peaks are strictly non-overlapping.[55-57] The peak partial overlap for cGNR can be assigned to a higher stability of the Br due to its interaction with the precursors, thus the HBr formation is slightly less favorable compared to H_2 formation and the HBr desorption peak is delayed. We performed a simulation of the desorption spectra of Fig. 6 with Kinetic Monte Carlo (KMC) methods by considering a simple desorption system with diffusing H species and immobile Br atoms. The simulation indeed suggests a higher activation barrier for HBr desorption, as compared to the case where the peaks are strictly non-overlapping (see SI Fig. S8).

On Au(111), the HBr desorption peak is measured at a temperature of 250 °C and occurs simultaneously with a minor H_2 desorption peak (Fig. 6b). This desorption is observed at a temperature much lower than the GNR formation (350 °C, as determined by STM) and indicates that partial dehydrogenation has occurred. Below and above this temperature, similar covalent polymers are observed by STM (see SI Fig. S7). The partially dehydrogenated polymer that is compatible with such unchanged STM imaging contrast corresponds to the intermediate state shown in Fig. 1e. Here, an additional C-C bond connects

the phenyls labelled 1 and 4 with the triphenylene core. The stoichiometry of the corresponding partial hydrogen release is related to a H:Br ratio of 2:1, thus the HBr desorption peak is accompanied by a much lower H_2 desorption peak. The two HBr and H_2 desorption peaks are perfectly overlapping (Fig. 6b), suggesting again a high stability of Br due to its interaction with the precursors, as revealed also by the KMC simulations (see SI Fig. S8). The latter shows a slightly lower stability of Br on Au(111) as compared to Ag(111). The full completion of the cyclodehydrogenation reaction on Au(111) and the GNR formation finally occurs at 350 °C as revealed by a second H_2 desorption peak and in agreement with the STM observations.

On Cu(111) no HBr desorption peak was observed (Fig. 6c). The cyclodehydrogenation reaction takes place at around 250 °C and is revealed by a H_2 desorption peak. On this surface, no sign of Br desorption was measured up to an annealing temperature of 500 °C, in agreement with the observation of adsorbed Br species in the vicinity of the GNR in the STM images (SI Fig. S3). This is also coherent with the formation of armchair GNR shown in previous work,[81] where the presence of adsorbed Br was confirmed by XPS after the completion of the cyclodehydrogenation reactions and the GNR formation. Our results thus confirm that, on Cu(111), Br does not recombine with as-released H and stays on the surface up to high annealing temperature. This behavior could be modelled by KMC simulations provided an activation barrier for HBr formation larger than 1.3 eV (see SI Fig. S8). Interestingly, it was shown previously that Br can be anyway removed from the metal surface in the form of HBr by bombarding with an atomic H flux at room temperature,[55,82-85] but in this case a low yield of ~10^{-3} per H atom[83] was estimated for HBr recombination. On copper surfaces, bromine is expected to leave the clean surface at higher annealing temperatures in the form of copper bromide.[86,87]

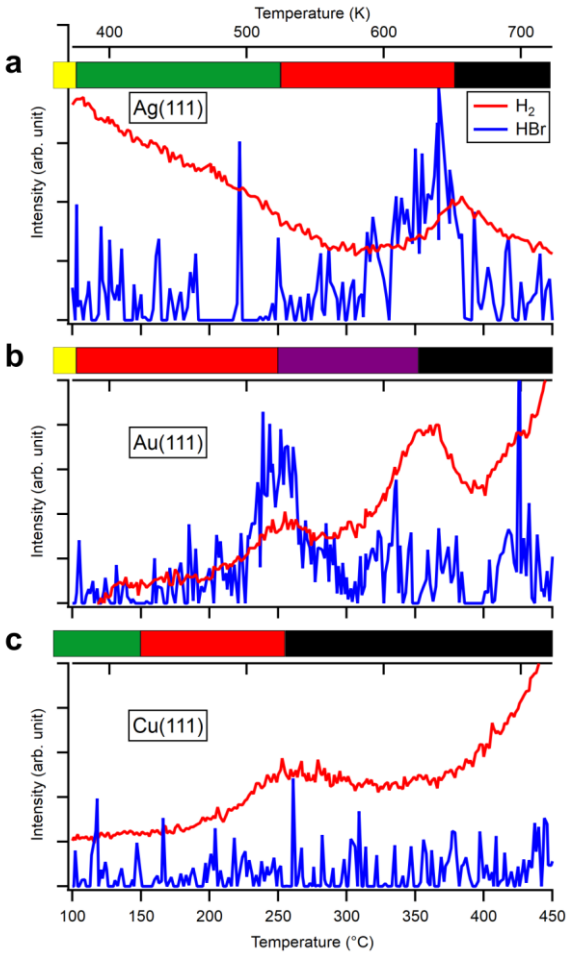

Fig. 6. Thermal desorption spectra (TDS) on (a) Ag(111), (b) Au(111), (c) Cu(111). Heating rate 20K/min. The signals are arbitrary scaled. The color bars refer to the different chemical structures as detailed in Fig. 1. The decreasing (resp. increasing) background signal at low (resp. high) temperature is due to degassing from the filament and the heating stage.

Discussion

In LT-STM images the adsorbed Br atoms are usually visualized in the form of individual bright dots[88] (SI Fig. S3), and in surface-supported Ullmann-like coupling reactions they often remain in the vicinity of the polymers after their release from the molecular precursors, as e.g. during the formation of polyphenylene chains.[46,83] In the case of aGNR obtained from dibromo-dianthracenyl precursors, the Br adatoms were never observed in STM images.[6,11,13,81] It was shown that for the intermediate poly-anthracenyl chains, the Br atoms preferentially sit under the protruding arm of the anthracenyl units[55] and thus become invisible to STM. Similarly, in the case of precursor **1**, on all surfaces the Br atoms were never observed in the organometallic chains and the covalent polymers (see Figs. 2,3). We can thus

expect Br to be sitting in close interaction with the protruding phenyls, and thus eventually to influence the cyclodehydrogenation process.

On the Ag(111) surface, Br can capture a H atom released by the cyclodehydrogenation and desorb in the form of HBr, and on Au(111) Br has already left the surface. On both Ag(111) and Au(111) the STM observations show that only neighboring 1,2 or 3,4 phenyl pairs react in the first step in a similar reaction pathway (Fig. 4d), thus suggesting that Br is not involved in the cyclodehydrogenation mechanism, and that the latter is intrinsic to the precursor. But on the Cu(111) surface, the cyclodehydrogenation takes place through a modified reaction pathway, involving first the two phenyls labelled 2,3 (see Fig. 4e). While Br does not participate in the global cyclodehydrogenation reaction as it remains afterwards on the surface, this observation suggests that nevertheless on Cu(111) the adsorbed Br has a certain influence on the reaction mechanism.

The similarity between the Ag(111) and Au(111) surfaces further suggests that, on Ag(111) also, the polymer intermediate state (Fig. 1e) is formed during the cyclodehydrogenation process, although short-lived and not observed.

During the cyclodehydrogenation reaction pathway, at a certain step, a noticeable stress is produced at the phenyl labelled 1 and 4 that can eventually give rise to their elimination and the creation of typical defects (Fig. S6). Because these defects are observed only on Ag(111) and Au(111), it is also suggested that the mechanism leading to their creation may be related to the formation of the polymer intermediate state of Fig. 1e. The proposed scenario for these different issues is however only speculative, and a detailed theoretical study would be necessary to elucidate the full cyclodehydrogenation mechanism.

Summary of the main issues observed during the growth of chevron GNR:

- The organometallic chains are not observed on Au(111), only on Ag(111) and Cu(111)
- Different kinds of interchain interactions are found depending on the degree of chain intertwining
- Partial dehydrogenation at an intermediate annealing temperature is found on Au(111)
- The cyclodehydrogenation mechanism occurs in a defined order, between the phenyls labelled 2,3 on Cu(111) and between those labelled 1,2 or 3,4 on Ag(111) and Au(111).
- A long-range repulsive interaction between the as-formed GNR leads to their distribution on the surface in mostly isolated form.
- In the STM images the Br atoms remain hidden behind the precursors during all steps before GNR formation

- In TDS, the HBr desorption peak is relatively delayed with respect to the H_2 desorption peak, thus revealing a high stability of Br in interaction with the precursors
- HBr desorption is not observed on Cu(111)

Conclusions

We have performed a systematic comparative study of the growth mechanism of chevron GNR on the Ag(111), Au(111) and Cu(111) surfaces. While on all surfaces the structure of the GNR remains qualitatively the same, noticeable differences are observed for the intermediate species appearing during the growth. The latter is a four-step process after the UHV deposition of the molecular precursor **1**: debromination, formation of organometallic chains, formation of covalent polymer chains and cyclodehydrogenation to produce the final fully aromatic planar GNR. No organometallic compound is observed on Au(111) as it is usually the case in Ullmann-like coupling reactions except in rare cases.[49,50] The organometallic and polymer chains organize in dense domains through lateral π-π interactions between the freely rotating phenyl groups of the precursors. They can be of different types, depending on the degree of chain intertwining. A partially dehydrogenated polymer was observed as an additional intermediate state on Au(111), as revealed by the HBr and H_2 desorption peaks measured in TDS at an intermediate annealing temperature. Two different mechanisms were found for the final cyclodehydrogenation step. The fusion between the four freely rotating phenyls of the precursor occurs first between the phenyls labelled 2 and 3 on Cu(111) and between those labelled 1 and 2, or 3 and 4 on Ag(111) and Au(111). An important long-range repulsive interaction is systematically observed after GNR formation leading to the transformation of the supramolecular domains into a distribution of well-separated GNRs. Before the GNR formation, the Br atoms released after the debromination of the precursors are adsorbed under the molecules and remain invisible by STM. The analysis of the TD spectra and their modelling by Kinetic Monte Carlo methods reveal a higher stability of the Br adsorbed state in this configuration. The Br desorbs from the surface during the dehydrogenation reaction in the form of HBr on Au(111) and Ag(111), but remains in an adsorbed state in close vicinity of the GNR on Cu(111).

Our results demonstrate that, due to its relative complexity with four freely rotating phenyl groups, precursor **1** can produce an important number of intermediate states and intriguing side effects along the pathway to chevron GNR formation. The precise chemical structure of the intermediate states should be considered carefully, depending on the nature of the supporting surface. In particular, the adsorption site of Br under the molecule and its role in the cyclodehydrogenation process still needs to be elucidated,

as well as the surface-dependent mechanism of the cyclodehydrogenation reaction. Finally, it is expected that similar or even more complex effects take place for other GNRs when large and flexible precursors are used.

Supporting Information

Additional STM images; Kinetic Monte Carlo simulations; additional details for methods.

Acknowledgments

The authors acknowledge Franck Para for experimental support, Frédéric Chérioux and Christian Wäckerlin for fruitful discussions, and Johan Lukkien for providing the CARLOS program. The project leading to this publication has received funding from the Agence Nationale de la Recherche (ANR Grant No. ANR-21-CE09-0025 ‘‘GANESH’’). This work has been supported by a public grant overseen by the French National Research Agency (ANR) as part of the "Investissements d’Avenir" program (Labex NanoSaclay, reference: ANR-10-LABX-0035).

References

(1) Clair, S.; De Oteyza, D. G. Controlling a Chemical Coupling Reaction on a Surface: Tools and Strategies for On-Surface Synthesis. *Chem. Rev.* **2019,** *119*, 4717-4776.

(2) Palmino, F.; Loppacher, C.; Cherioux, F. Photochemistry Highlights on On-Surface Synthesis. *ChemPhysChem* **2019,** *20*, 2271-2280.

(3) Grill, L.; Hecht, S. Covalent on-surface polymerization. *Nat. Chem.* **2020,** *12*, 115-130.

(4) Lackinger, M. Synthesis on inert surfaces. *Dalton Transactions* **2021,** *50*, 10020-10027.

(5) Stolza, S.; Di Giovannantonio, M.; Groning, O.; Widmer, R. On-surface Synthesis: What Happens Behind the Scenes? *Chimia* **2022,** *76*, 203-211.

(6) Cai, J. M.; Ruffieux, P.; Jaafar, R.; Bieri, M.; Braun, T.; Blankenburg, S.; Muoth, M.; Seitsonen, A. P.; Saleh, M.; Feng, X.; et al. Atomically Precise Bottom-Up Fabrication of Graphene Nanoribbons. *Nature* **2010,** *466*, 470-473.

(7) Zhou, X. H.; Yu, G. Modified Engineering of Graphene Nanoribbons Prepared via On-Surface Synthesis. *Adv. Mater.* **2020,** *32*, 1905957.

(8) Talirz, L.; Ruffieux, P.; Fasel, R. On-Surface Synthesis of Atomically Precise Graphene Nanoribbons. *Adv. Mater.* **2016,** *28*, 6222-6231.

(9) Houtsma, R. S. K.; de la Rie, J.; Stohr, M. Atomically precise graphene nanoribbons: interplay of structural and electronic properties. *Chem. Soc. Rev.* **2021,** *50*, 6541-6568.

(10) Corso, M.; Carbonell-Sanromà, E.; de Oteyza, D. G., Bottom-Up Fabrication of Atomically Precise Graphene Nanoribbons, In *On-Surface Synthesis II* Springer International Publishing: Cham, **2018**; p 113-152.

(11) Simonov, K. A.; Vinogradov, N. A.; Vinogradov, A. S.; Generalov, A. V.; Zagrebina, E. M.; Svirskiy, G. I.; Cafolla, A. A.; Carpy, T.; Cunniffe, J. P.; Taketsugu, T.; et al. From Graphene Nanoribbons on Cu(111) to Nanographene on Cu(110): Critical Role of Substrate Structure in the Bottom-Up Fabrication Strategy. *ACS Nano* **2015,** *9*, 8997-9011.

(12) Moreno, C.; Panighel, M.; Vilas-Varela, M.; Sauthier, G.; Tenorio, M.; Ceballos, G.; Pena, D.; Mugarza, A. Critical Role of Phenyl Substitution and Catalytic Substrate in the Surface-Assisted Polymerization of Dibromobianthracene Derivatives. *Chem. Mater.* **2019,** *31*, 331-341.

(13) Simonov, K. A.; Generalov, A. V.; Vinogradov, A. S.; Svirskiy, G. I.; Cafolla, A. A.; McGuinness, C.; Taketsugu, T.; Lyalin, A.; Mårtensson, N.; Preobrajenski, A. B. Synthesis of Armchair Graphene Nanoribbons from the 10,10'-Dibromo-9,9′ -Bianthracene Molecules on Ag(111): the Role of Organometallic Intermediates. *Sci. Rep.* **2018,** *8*, 3506.

(14) Vo, T. H.; Shekhirev, M.; Kunkel, D. A.; Morton, M. D.; Berglund, E.; Kong, L. M.; Wilson, P. M.; Dowben, P. A.; Enders, A.; Sinitskii, A. Large-Scale Solution Synthesis of Narrow Graphene Nanoribbons. *Nat. Commun.* **2014,** *5*, 3189.

(15) Pereira, M. L.; da Cunha, W. F.; de Sousa, R. T.; Giozza, W. F.; Silva, G. M. E.; Ribeiro, L. A. Charge Transport Mechanism in Chevron-Graphene Nanoribbons. *J. Phys. Chem. C* **2020,** *124*, 22392-22398.

(16) Deniz, O.; Sanchez-Sanchez, C.; Jaafar, R.; Kharche, N.; Liang, L.; Meunier, V.; Feng, X.; Mullen, K.; Fasel, R.; Ruffieux, P. Electronic Characterization of Silicon Intercalated Chevron Graphene Nanoribbons on Au(111). *Chem. Commun.* **2018,** *54*, 1619-1622.

(17) Teeter, J. D.; Costa, P. S.; Pour, M. M.; Miller, D. P.; Zurek, E.; Enders, A.; Sinitskii, A. Epitaxial growth of aligned atomically precise chevron graphene nanoribbons on Cu(111). *Chem. Commun.* **2017,** *53*, 8463-8466.

(18) Radocea, A.; Sun, T.; Vo, T. H.; Sinitskii, A.; Aluru, N. R.; Lyding, J. W. Solution-Synthesized Chevron Graphene Nanoribbons Exfoliated onto H:Si(100). *Nano Lett.* **2017,** *17*, 170-178.

(19) Galeotti, G.; Fritton, M.; Lischka, M.; Obermann, S.; Ma, J.; Heckl, W. M.; Feng, X.; Lackinger, M. Initial Coupling and Reaction Progression of Directly Deposited Biradical Graphene Nanoribbon Monomers on Iodine-Passivated Versus Pristine Ag(111). *Chemistry* **2022,** *4*, 259-269.

(20) Dobner, C.; Li, G.; Sarker, M.; Sinitskii, A.; Enders, A. Diffusion-controlled on-surface synthesis of graphene nanoribbon heterojunctions. *RSC Adv.* **2022,** *12*, 6615-6618.

(21) Lv, Y. W.; Ye, S. Z.; Wang, H.; He, J.; Huang, Q. J.; Chang, S. Strain engineering of chevron graphene nanoribbons. *J. Appl. Phys.* **2019,** *125*, 082501.

(22) Linden, S.; Zhong, D.; Timmer, A.; Aghdassi, N.; Franke, J. H.; Zhang, H.; Feng, X.; Mullen, K.; Fuchs, H.; Chi, L.; et al. Electronic Structure of Spatially Aligned Graphene Nanoribbons on Au(788). *Phys. Rev. Lett.* **2012,** *108*, 216801.

(23) Bronner, C.; Marangoni, T.; Rizzo, D. J.; Durr, R. A.; Jorgensen, J. H.; Fischer, F. R.; Crommie, M. F. Iodine versus Bromine Functionalization for Bottom-Up Graphene Nanoribbon Growth: Role of Diffusion. *J. Phys. Chem. C* **2017,** *121*, 18490-18495.

(24) Teeter, J. D.; Costa, P. S.; Zahl, P.; Vo, T. H.; Shekhirev, M.; Xu, W. W.; Zeng, X. C.; Enders, A.; Sinitskii, A. Dense Monolayer Films of Atomically Precise Graphene Nanoribbons on Metallic Substrates Enabled by Direct Contact Transfer of Molecular Precursors. *Nanoscale* **2017,** *9*, 18835-18844.

(25) Teeter, J. D.; Zahl, P.; Pour, M. M.; Costa, P. S.; Enders, A.; Sinitskii, A. On-Surface Synthesis and Spectroscopic Characterization of Laterally Extended Chevron Graphene Nanoribbons. *ChemPhysChem* **2019,** *20*, 2281-2285.

(26) Cernevics, K.; Yazyev, O. V. From defect to effect: controlling electronic transport in chevron graphene nanoribbons. *Electronic Structure* **2023,** *5*, 014006.

(27) Costa, P. S.; Teeter, J. D.; Enders, A.; Sinitskii, A. Chevron-Based Graphene Nanoribbon Heterojunctions: Localized Effects of Lateral Extension and Structural Defects on Electronic Properties. *Carbon* **2018,** *134*, 310-315.

(28) Chen, Z. P.; Zhang, W.; Palma, C. A.; Rizzini, A. L.; Liu, B. L.; Abbas, A.; Richter, N.; Martini, L.; Wang, X. Y.; Cavani, N.; et al. Synthesis of Graphene Nanoribbons by Ambient-Pressure Chemical Vapor Deposition and Device Integration. *J. Am. Chem. Soc.* **2016,** *138*, 15488-15496.

(29) Cai, J. M.; Pignedoli, C. A.; Talirz, L.; Ruffieux, P.; Sode, H.; Liang, L. B.; Meunier, V.; Berger, R.; Li, R. J.; Feng, X. L.; et al. Graphene Nanoribbon Heterojunctions. *Nat. Nanotechnol.* **2014,** *9*, 896-900.

(30) Azevedo, A. S. D.; Saraiva-Souza, A.; Meunier, V.; Girao, E. C. Electronic properties of N-rich graphene nano-chevrons. *Phys. Chem. Chem. Phys.* **2021,** *23*, 13204-13215.

(31) Maass, F.; Utecht, M.; Stremlau, S.; Gille, M.; Schwarz, J.; Hecht, S.; Klamroth, T.; Tegeder, P. Electronic structure changes during the on-surface synthesis of nitrogen-doped chevron-shaped graphene nanoribbons. *Phys. Rev. B* **2017,** *96*, 045434.

(32) Lv, Y. W.; Huang, Q. J.; Chang, S.; Wang, H.; He, J.; Liu, A. Q.; Ye, S. Z.; Wang, W. Activating impurity effect in edge nitrogen-doped chevron graphene nanoribbons. *Journal of Physics Communications* **2018,** *2*, 045028.

(33) Cao, Y.; Qi, J.; Zhang, Y.-F.; Huang, L.; Zheng, Q.; Lin, X.; Cheng, Z.; Zhang, Y.-Y.; Feng, X.; Du, S.; et al. Tuning the Morphology of Chevron-Type Graphene Nanoribbons by Choice of Annealing Temperature. *Nano Res.* **2018,** *11*, 6190-6196.

(34) Wen, E. C. H.; Jacobse, P. H.; Jiang, J. W.; Wang, Z. Y.; McCurdy, R. D.; Louie, S. G.; Crommie, M. F.; Fischer, F. R. Magnetic Interactions in Substitutional Core-Doped Graphene Nanoribbons. *J. Am. Chem. Soc.* **2022,** *144*, 13696-13703.

(35) Marquez, I. R.; del Arbol, N. R.; Urgel, J. I.; Villalobos, F.; Fasel, R.; Lopez, M. F.; Cuerva, J. M.; Martin-Gago, J. A.; Campana, A. G.; Sanchez-Sanchez, C. On-Surface Thermal Stability of a Graphenic Structure Incorporating a Tropone Moiety. *Nanomaterials* **2022,** *12*, 488.

(36) Bronner, C.; Stremlau, S.; Gille, M.; Brausse, F.; Haase, A.; Hecht, S.; Tegeder, P. Aligning the Band Gap of Graphene Nanoribbons by Monomer Doping. *Angew. Chem. Int. Ed.* **2013,** *52*, 4422-4425.

(37) Zhang, Y.; Zhang, Y. F.; Li, G.; Lu, J. C.; Lin, X.; Du, S. X.; Berger, R.; Feng, X. L.; Müllen, K.; Gao, H. J. Direct visualization of atomically precise nitrogen-doped graphene nanoribbons. *Appl. Phys. Lett.* **2014,** *105*, 023101.

(38) Vo, T. H.; Shekhirev, M.; Kunkel, D. A.; Orange, F.; Guinel, M. J. F.; Enders, A.; Sinitskii, A. Bottom-up solution synthesis of narrow nitrogen-doped graphene nanoribbons. *Chem. Commun.* **2014,** *50*, 4172-4174.

(39) Shekhirev, M.; Zahl, P.; Sinitskii, A. Phenyl Functionalization of Atomically Precise Graphene Nanoribbons for Engineering Inter-ribbon Interactions and Graphene Nanopores. *ACS Nano* **2018,** *12*, 8662-8669.

(40) Jacobse, P. H.; McCurdy, R. D.; Jiang, J. W.; Rizzo, D. J.; Veber, G.; Butler, P.; Zuzak, R.; Louie, S. G.; Fischer, F. R.; Crommie, M. F. Bottom-up Assembly of Nanoporous Graphene with Emergent Electronic States. *J. Am. Chem. Soc.* **2020,** *142*, 13507-13514.

(41) Mutlu, Z.; Jacobse, P. H.; McCurdy, R. D.; Llinas, J. P.; Lin, Y. X.; Veber, G. C.; Fischer, F. R.; Crommie, M. F.; Bokor, J. Bottom-Up Synthesized Nanoporous Graphene Transistors. *Adv. Funct. Mater.* **2021,** *31*, 2103798.

(42) Nguyen, G. D.; Tsai, H. Z.; Omrani, A. A.; Marangoni, T.; Wu, M.; Rizzo, D. J.; Rodgers, G. F.; Cloke, R. R.; Durr, R. A.; Sakai, Y.; et al. Atomically precise graphene nanoribbon heterojunctions from a single molecular precursor. *Nat. Nanotechnol.* **2017,** *12*, 1077-1082.

(43) Durr, R. A.; Haberer, D.; Lee, Y. L.; Blackwell, R.; Kalayjian, A. M.; Marangoni, T.; Ihm, J.; Louie, S. G.; Fischer, F. R. Orbitally Matched Edge-Doping in Graphene Nanoribbons. *J. Am. Chem. Soc.* **2018,** *140*, 807-813.

(44) Bronner, C.; Durr, R. A.; Rizzo, D. J.; Lee, Y.-L.; Marangoni, T.; Kalayjian, A. M.; Rodriguez, H.; Zhao, W.; Louie, S. G.; Fischer, F. R.; et al. Hierarchical On-Surface Synthesis of Graphene Nanoribbon Heterojunctions. *ACS Nano* **2018,** *12*, 2193-2200.

(45) Dong, L.; Wang, S.; Wang, W.; Chen, C.; Lin, T.; Adisoejoso, J.; Lin, N., Transition Metals Trigger On-Surface Ullmann Coupling Reaction: Intermediate, Catalyst and Template, In *On-Surface Synthesis*; Springer-Verlag: Berlin, **2016**; p 23-42.

(46) Ivanovskaya, V. V.; Zobelli, A.; Basagni, A.; Casalini, S.; Colazzo, L.; de Boni, F.; Oteyza, D.; Sambi, M.; Sedona, F. On-Surface Synthesis and Evolution of Self-Assembled Poly(p-phenylene) Chains on Ag(111): A Joint Experimental and Theoretical Study. *J. Phys. Chem. C* **2023,** *127*, 393-402.

(47) Shi, K. J.; Yuan, D. W.; Wang, C. X.; Shu, C. H.; Li, D. Y.; Shi, Z. L.; Wu, X. Y.; Liu, P. N. Ullmann Reaction of Aryl Chlorides on Various Surfaces and the Application in Stepwise Growth of 2D Covalent Organic Frameworks. *Org. Lett.* **2016,** *18*, 1282-1285.

(48) Jung, J.; Mollenhauer, D. Theoretical Studies of the Mechanism of Ullmann Coupling of Naphthyl Halogen Derivatives to Binaphtyl on Coinage Metals. *J. Phys. Chem. C* **2023,** *127*, 20284-20300.

(49) Berdonces-Layunta, A.; Schulz, F.; Aguilar-Galindo, F.; Lawrence, J.; Mohammed, M. S. G.; Muntwiler, M.; Lobo-Checa, J.; Liljeroth, P.; de Oteyza, D. G. Order from a Mess: The Growth of 5-Armchair Graphene Nanoribbons. *ACS Nano* **2021,** *15*, 16552-16561.

(50) Barin, G. B.; Sun, Q.; Di Giovannantonio, M.; Du, C. Z.; Wang, X. Y.; Llinas, J. P.; Mutlu, Z.; Lin, Y. X.; Wilhelm, J.; Overbeck, J.; et al. Growth Optimization and Device Integration of Narrow-Bandgap Graphene Nanoribbons. *Small* **2022,** *18*, 2202301.

(51) Smerieri, M.; Pis, I.; Ferrighi, L.; Nappini, S.; Lusuan, A.; Di Valentin, C.; Vaghi, L.; Papagni, A.; Cattelan, M.; Agnoli, S.; et al. Synthesis of graphene nanoribbons with a defined mixed edge-site sequence by surface assisted polymerization of (1,6)-dibromopyrene on Ag(110). *Nanoscale* **2016,** *8*, 17843-17853.

(52) Di Giovannantonio, M.; Deniz, O.; Urgel, J. I.; Widmer, R.; Dienel, T.; Stolz, S.; Sanchez-Sanchez, C.; Muntwiler, M.; Dumslaff, T.; Berger, R.; et al. On-Surface Growth Dynamics of Graphene Nanoribbons: The Role of Halogen Functionalization. *ACS Nano* **2018,** *12*, 74-81.

(53) Mairena, A.; Wienke, M.; Martin, K.; Avarvari, N.; Terfort, A.; Ernst, K. H.; Wäckerlin, C. Stereospecific Autocatalytic Surface Explosion Chemistry of Polycyclic Aromatic Hydrocarbons. *J. Am. Chem. Soc.* **2018,** *140*, 7705-7709.

(54) Reocreux, R.; Kress, P. L.; Hannagan, R. T.; Cinar, V.; Stamatakis, M.; Sykes, E. C. H. Controlling Hydrocarbon (De)Hydrogenation Pathways with Bifunctional PtCu Single-Atom Alloys. *J. Phys. Chem. Lett.* **2020,** *11*, 8751-8757.

(55) Bronner, C.; Bjork, J.; Tegeder, P. Tracking and Removing Br during the On-Surface Synthesis of a Graphene Nanoribbon. *J. Phys. Chem. C* **2015,** *119*, 486-493.

(56) Thussing, S.; Flade, S.; Eimre, K.; Pignedoli, C. A.; Fasel, R.; Jakob, P. Reaction Pathway toward Seven-Atom-Wide Armchair Graphene Nanoribbon Formation and Identification of Intermediate Species on Au(111). *J. Phys. Chem. C* **2020,** *124*, 16009-16018.

(57) Mairena, A.; Baljozovic, M.; Kawecki, M.; Grenader, K.; Wienke, M.; Martin, K.; Bernard, L.; Avarvari, N.; Terfort, A.; Ernst, K. H.; et al. The Fate of Bromine after Temperature-Induced Dehydrogenation of On-Surface Synthesized Bisheptahelicene. *Chem. Sci.* **2019,** *10*, 2998-3004.

(58) Saleh, M.; Baumgarten, M.; Mavrinskiy, A.; Schafer, T.; Mullen, K. Triphenylene-Based Polymers for Blue Polymeric Light Emitting Diodes. *Macromolecules* **2010,** *43*, 137-143.

(59) Horcas, I.; Fernández, R.; Gómez-Rodríguez, J. M.; Colchero, J.; Gómez-Herrero, J.; Baro, A. M. WSXM: A software for scanning probe microscopy and a tool for nanotechnology. *Rev. Sci. Inst.* **2007,** *78*, 013705.

(60) Lukkien, J. J.; Segers, J. P. L.; Hilbers, P. A. J.; Gelten, R. J.; Jansen, A. P. J. Efficient Monte Carlo methods for the simulation of catalytic surface reactions. *Phys. Rev. E* **1998,** *58*, 2598-2610.

(61) Lukkien, J. J.; Jansen, A. P. J., CARLOS version 5.2, http://carlos.win/tue/nl; Eindhoven University of Technology, Eindhoven, **2009**.

(62) Ajayakumar, M. R.; Di Giovannantonio, M.; Pignedoli, C. A.; Yang, L.; Ruffieux, P.; Ma, J.; Fasel, R.; Feng, X. L. On-surface synthesis of porous graphene nanoribbons containing nonplanar [14]annulene pores. *J. Polym. Sci.* **2022,** *60*, 1912-1917.

(63) Blankenburg, S.; Cai, J. M.; Ruffieux, P.; Jaafar, R.; Passerone, D.; Feng, X. L.; Mullen, K.; Fasel, R.; Pignedoli, C. A. Intraribbon Heterojunction Formation in Ultranarrow Graphene Nanoribbons. *ACS Nano* **2012,** *6*, 2020-2025.

(64) Treier, M.; Pignedoli, C. A.; Laino, T.; Rieger, R.; Mullen, K.; Passerone, D.; Fasel, R. Surface-Assisted Cyclodehydrogenation Provides a Synthetic Route Towards Easily Processable and Chemically Tailored Nanographenes. *Nat. Chem.* **2011,** *3*, 61-67.

(65) Wang, X. Y.; Dienel, T.; Di Giovannantonio, M.; Barin, G. B.; Kharche, N.; Deniz, O.; Urgel, J. I.; Widmer, R.; Stolz, S.; De Lima, L. H.; et al. Heteroatom-Doped Perihexacene from a Double Helicene Precursor: On-Surface Synthesis and Properties. *J. Am. Chem. Soc.* **2017,** *139*, 4671-4674.

(66) Moreno, C.; Paradinas, M.; Vilas-Varela, M.; Panighel, M.; Ceballos, G.; Pena, D.; Mugarza, A. On-Surface Synthesis of Superlattice Arrays of Ultra-Long Graphene Nanoribbons. *Chem. Commun.* **2018,** *54*, 9402.

(67) Talirz, L.; Sode, H.; Dumslaff, T.; Wang, S. Y.; Sanchez-Valencia, J. R.; Liu, J.; Shinde, P.; Pignedoli, C. A.; Liang, L. B.; Meunier, V.; et al. On-Surface Synthesis and Characterization of 9-Atom Wide Armchair Graphene Nanoribbons. *ACS Nano* **2017,** *11*, 1380-1388.

(68) Forker, R.; Peuker, J.; Meissner, M.; Sojka, F.; Ueba, T.; Yamada, T.; Kato, H. S.; Munakata, T.; Fritz, T. The Complex Polymorphism and Thermodynamic Behavior of a Seemingly Simple System: Naphthalene on Cu(111). *Langmuir* **2014,** *30*, 14163-14170.

(69) Soubatch, S.; Kröger, I.; Kumpf, C.; Tautz, F. S. Structure and growth of tetracene on Ag(111). *Phys. Rev. B* **2011,** *84*, 195440.

(70) Bobrov, K.; Kalashnyk, N.; Guillemot, L. True perylene epitaxy on Ag(110) driven by site recognition effect. *J. Chem. Phys.* **2015,** *142*, 101929.

(71) Huempfner, T.; Sojka, F.; Forker, R.; Fritz, T. Growth of coronene on (100)- and (111)-surfaces of fcc-crystals. *Surf. Sci.* **2015,** *639*, 80-88.

(72) Wagner, C.; Kasemann, D.; Golnik, C.; Forker, R.; Esslinger, M.; Müllen, K.; Fritz, T. Repulsion between molecules on a metal: Monolayers and submonolayers of hexa-*peri*-hexabenzocoronene on Au(111). *Phys. Rev. B* **2010,** *81*, 035423.

(73) Bischoff, F.; Seufert, K.; Auwärter, W.; Joshi, S.; Vijayaraghavan, S.; Écija, D.; Diller, K.; Papageorgiou, A. C.; Fischer, S.; Allegretti, F.; et al. How Surface Bonding and Repulsive Interactions Cause Phase Transformations: Ordering of a Prototype Macrocyclic Compound on Ag(111). *ACS Nano* **2013,** *7*, 3139-3149.

(74) Fernandez-Torrente, I.; Monturet, S.; Franke, K. J.; Fraxedas, J.; Lorente, N.; Pascual, J. I. Long-Range Repulsive Interaction between Molecules on a Metal Surface Induced by Charge Transfer. *Phys. Rev. Lett.* **2007,** *99*, 176103.

(75) Rojas, G.; Simpson, S.; Chen, X. M.; Kunkel, D. A.; Nitz, J.; Xiao, J.; Dowben, P. A.; Zurek, E.; Enders, A. Surface state engineering of molecule-molecule interactions. *Phys. Chem. Chem. Phys.* **2012,** *14*, 4971-4976.

(76) Kawai, S.; Benassi, A.; Gnecco, E.; Sode, H.; Pawlak, R.; Feng, X. L.; Mullen, K.; Passerone, D.; Pignedoli, C. A.; Ruffieux, P.; et al. Superlubricity of Graphene Nanoribbons on Gold Surfaces. *Science* **2016,** *351*, 957-961.

(77) Ohtomo, M.; Hayashi, H.; Shiotari, A.; Kawamura, M.; Hayashi, R.; Jippo, H.; Yamaguchi, J.; Ohfuchi, M.; Aratani, N.; Sugimoto, Y.; et al. On-surface synthesis of hydroxy-functionalized graphene nanoribbons through deprotection of methylenedioxy groups. *Nanoscale Adv.* **2022,** *4*, 4871-4879.

(78) De Boni, F.; Merlin, G.; Sedona, F.; Casalini, S.; Fakhrabadi, M. M. S.; Sambi, M. Templating Effect of Different Low-Miller-Index Gold Surfaces on the Bottom-Up Growth of Graphene Nanoribbons. *Acs Applied Nano Materials* **2020,** *3*, 11497-11509.

(79) Merino-Diez, N.; Lobo-Checa, J.; Nita, P.; Garcia-Lekue, A.; Basagni, A.; Vasseur, G.; Tiso, F.; Sedona, F.; Das, P. K.; Fujii, J.; et al. Switching from Reactant to Substrate Engineering in the Selective Synthesis of Graphene Nanoribbons. *J. Phys. Chem. Lett.* **2018,** *9*, 2510-2517.

(80) Fritton, M.; Duncan, D. A.; Deimel, P. S.; Rastgoo-Lahrood, A.; Allegretti, F.; Barth, J. V.; Heckl, W. M.; Bjork, J.; Lackinger, M. The Role of Kinetics versus Thermodynamics in Surface-Assisted Ullmann Coupling on Gold and Silver Surfaces. *J. Am. Chem. Soc.* **2019,** *141*, 4824-4832.

(81) Simonov, K. A.; Vinogradov, N. A.; Vinogradov, A. S.; Generalov, A. V.; Zagrebina, E. M.; Martensson, N.; Cafolla, A. A.; Carpy, T.; Cunniffe, J. P.; Preobrajenski, A. B. Effect of Substrate Chemistry on the Bottom-Up Fabrication of Graphene Nanoribbons: Combined Core-Level Spectroscopy and STM Study. *J. Phys. Chem. C* **2014,** *118*, 12532-12540.

(82) Enderson, Z. A.; Murali, H.; Dasari, R. R.; Dai, Q. Q.; Li, H.; Parker, T. C.; Bredas, J. L.; Marder, S. R.; First, P. N. Tailoring On-Surface Molecular Reactions and Assembly through Hydrogen-Modified Synthesis: From Triarylamine Monomer to 2D Covalent Organic Framework. *ACS Nano* **2023,** *17*, 7366–7376.

(83) Abyazisani, M.; MacLeod, J. M.; Lipton-Duffin, J. Cleaning up after the Party: Removing the Byproducts of On-Surface Ullmann Coupling. *ACS Nano* **2019,** *13*, 9270-9278.

(84) Zuzak, R.; Jancarik, A.; Gourdon, A.; Szymonski, M.; Godlewski, S. On-Surface Synthesis with Atomic Hydrogen. *ACS Nano* **2020,** *14*, 13316-13323.

(85) Tran, B. V.; Pham, T. A.; Grunst, M.; Kivala, M.; Stohr, M. Surface-Confined [2+2] Cycloaddition Towards One-Dimensional Polymers Featuring Cyclobutadiene Units. *Nanoscale* **2017,** *9*, 18305-18310.

(86) Nakakura, C. Y.; Altman, E. I. Bromine adsorption, reaction, and etching of Cu(100). *Surf. Sci.* **1997,** *370*, 32-46.

(87) Andryushechkin, B. V.; Pavlova, T. V.; Eltsov, K. N. Adsorption of halogens on metal surfaces. *Surf. Sci. Rep.* **2018,** *73*, 83-115.

(88) Dou, W. Z.; Wu, M. M.; Song, B. Y.; Zhi, G. X.; Hua, C. Q.; Zhou, M.; Niu, T. C. High-Yield Production of Quantum Corrals in a Surface Reconstruction Pattern. *Nano Lett.* **2023,** *23*, 148-154.

TOC Graphic

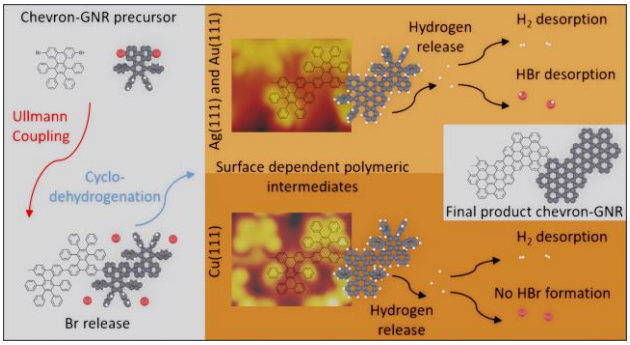
Chevron-GNR precursor
Ullmann Coupling
Cyclo-dehydrogenation
Br release
Ag(111) and Au(111)
Hydrogen release
H_2 desorption
HBr desorption
Surface dependent polymeric intermediates
Final product chevron-GNR
Cu(111)
H_2 desorption
No HBr formation
Hydrogen release